Desalination 548 (2023) 116255

Contents lists available at ScienceDirect

Desalination

journal homepage: www.elsevier.com/locate/desal

Nanorod-interlayered thin film composite membranes for ultrafast nanofiltration

Pengfei Li [a,b,c], Bingxin Wei [b], Zhen Yao [c], Peng Li [b], Yingfei Hou [b], Yang Yang [c,*], Q. Jason Niu [a,b,**]

[a] Institute for Advanced Study, Shenzhen University, Shenzhen 518060, PR China
[b] College of Chemical Engineering, China University of Petroleum (East China), Qingdao 266580, PR China
[c] Physics of Supramolecular Systems and Surfaces, Faculty of Physics, Bielefeld University, 33615 Bielefeld, Germany

HIGHLIGHTS

- A high-performance i-TFC membrane was fabricated by the IFIP on commercial hydrophobic substrates (PP, PE and PTFE).
- The i-TFC membrane showed high water permeance up to 48.9 $L{\cdot}m^{-2}{\cdot}h^{-1}{\cdot}bar^{-1}$ while maintaining high Na_2SO_4 rejection of 98.6%.
- The presence of FeOOH nanorods enhanced the water permeance, mechanical strength, and anti-fouling performance of the i-TFC membranes.

GRAPHICAL ABSTRACT

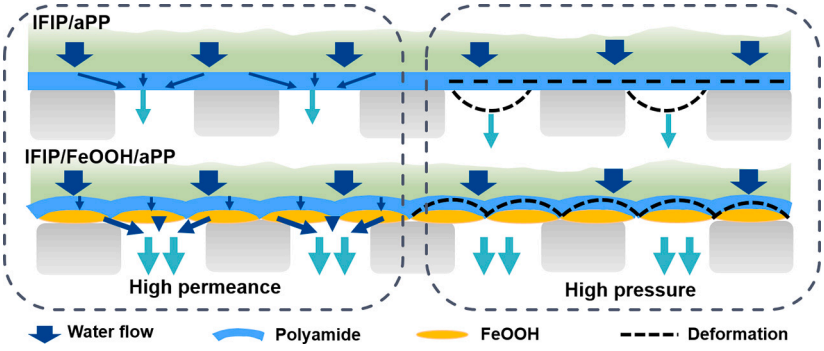

ARTICLE INFO

Keywords:
Nanofiltration
FeOOH
Hydrophobic-based membranes
Nanorod morphology
Polyamide membrane

ABSTRACT

Customizing high-performance nanofiltration membranes that can break the trade-off effect is critical to the development of membrane separation. Building an intermediate layer between the support and the selective layer to accelerate water transport is considered to be an effective solution to this issue. However, the synthesis of interlayered thin-film composite membranes (i-TFCs) on non-polar substrates with large pores and high porosity remains challenging. Here, we report a high-performance i-TFC membrane with FeOOH nanorods as interlayers. The porous and robust nanorods greatly increased the water transport paths and the mechanical strength of the membrane. Under the high pressure of 20 bar, the i-TFC membrane still remained a high salt rejection above 96 % while showing a high pure water permeance up to 48.9 $L{\cdot}m^{-2}{\cdot}h^{-1}{\cdot}bar^{-1}$. Furthermore, the presence of nanorods enhanced the hydrophilicity and compactness of the substrate, leading to the formation of a 23-nm thick polyamide layer without nanorod structures. The versatility of the strategy was also demonstrated with three different hydrophobic substrates. This work will thus provide further insights into the development of high-performance membranes for molecular separations.

* Corresponding author.
** Correspondence to: Q.J. Niu, Institute for Advanced Study, Shenzhen University, Shenzhen 518060, PR China.
E-mail addresses: yyang@physik.uni-bielefeld.de (Y. Yang), qjasonniu@szu.edu.cn (Q.J. Niu).

https://doi.org/10.1016/j.desal.2022.116255
Received 16 August 2022; Received in revised form 26 October 2022; Accepted 13 November 2022
Available online 26 November 2022

1. Introduction

The global water crisis drives the development of energy-efficient water treatment technologies [1,2]. Nanofiltration (NF) is an efficient separation process that utilizes nanopores of 1–10 nm for various liquid separations, such as water softening by repelling divalent ions [3,4]. The commercialized NF membrane is typically thin-film composite (TFC) consisting of a macroporous substrate as the support and a dense polyamide (PA) film as the selective layer. However, the TFC membrane often suffers from a trade-off effect between permeability and selectivity [5,6].

Recent breakthroughs in materials science have led to the development of membranes to break the bottleneck [7–10]. An effective strategy is to build a nanoporous interlayer between the support and the polyamide layer to accelerate water transport [11]. The interlayer can modulate the surface chemistry and pore structure, thereby effectively reducing the transport resistance and enabling fast transport of water molecules [12–14]. Furthermore, it advances the interfacial polymerization process to form a continuous dense polyamide film that combines high permeability and selectivity [15,16]. Meanwhile, the interlayer also improved the structural stability in resulted TFC membranes through the following two aspects. On the one hand, by strengthening the adhesion between the interlayer and both the polyamide layer and substrate. Wu et al. [17] deposited PDA coated COF as an interlayer for enhancement of structural stability simultaneously. The as-prepared PA/PDA-COF/PAN membrane maintained excellent stability compared with the control membrane in a 16-day solvent immersion experiment. On the other hand, by constructing a rigid interlayer, the mechanical properties of the skin layer of the support can be improved to enhance the pressure resistance of the TFC membrane. Hoek et al. [18] introduced nanoparticles of different sizes to increase the mechanical properties of the PSF, which in turn reduced the flux attenuation of the composite membrane during high-pressure testing. These advantageous characters have inspired numerous research on materials that can be utilized for interlayer fabrication, such as metal-organic frameworks, graphene oxide, covalent organic frameworks and carbon nanotubes [19–21]. However, these materials are mostly produced by vacuum filtration, which are difficult to scale up and also facing challenges of nanomaterial agglomeration and stability issues. Alternatively, interlayers such as Noria-polyethyleneimine and dendrimer that are highly compatible with polyamide have been developed [22,23]. However, synthesizing the precursors for these materials is a challenging step, and the stability of the polyamide layer is also sacrificed due to the formation of rough folded structures. In addition, attempts have been made to in-situ synthesize nanoparticles such as ZIF-8 interlayer on the support layer [24], but the use of ZIF-8 nanocrystals is constrained by their instability in water, especially for practical applications of high flux NF membranes.

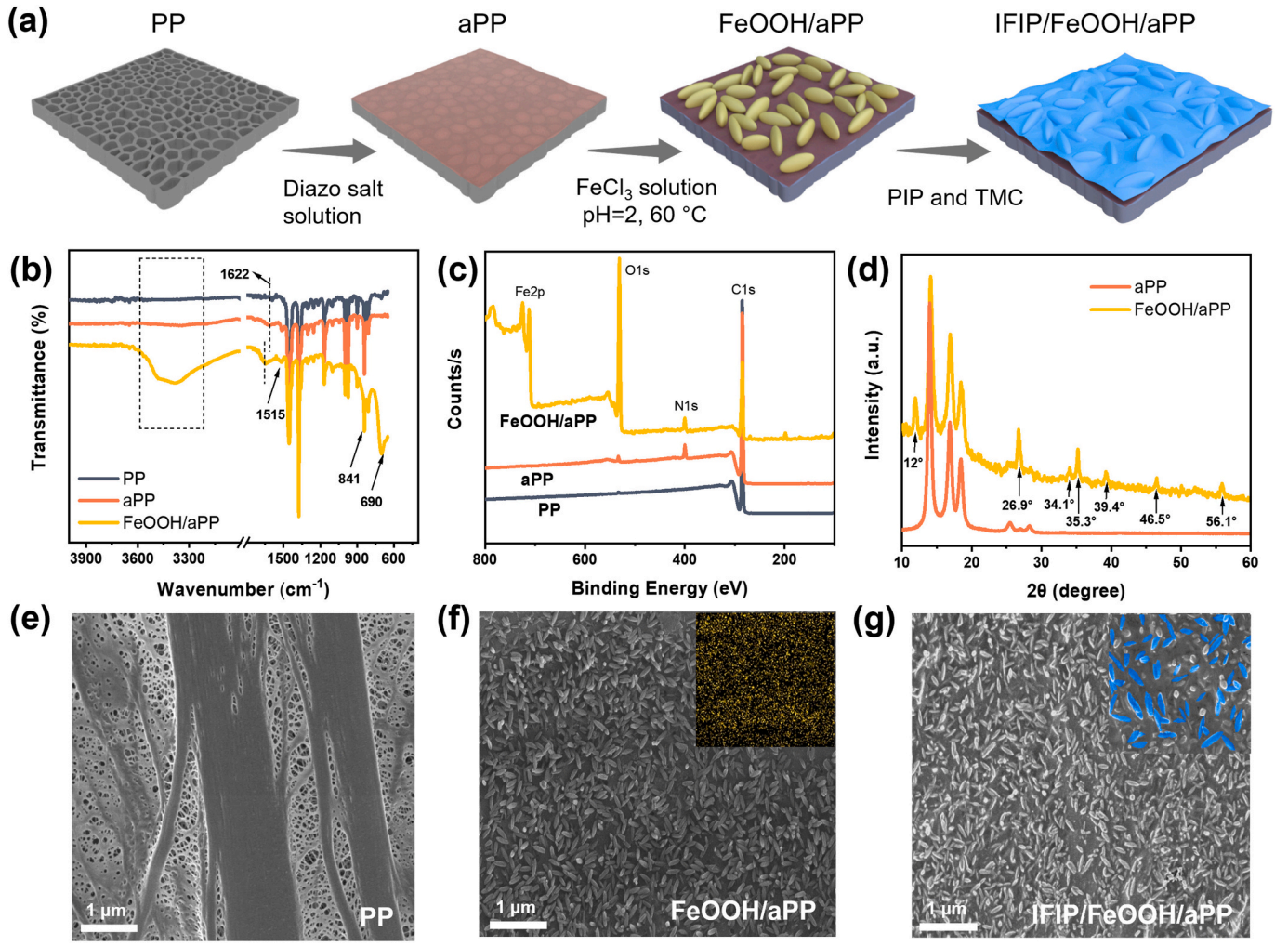

Fig. 1. (a) Schematic illustration of the fabrication process of the i-TFC membrane. (b) ATR-FTIR spectra; (c) XPS spectra and (d) XRD patterns of various membranes. SEM topography images of the (e) PP, (f) FeOOH/aPP (The inset picture (5 μm × 5 μm) is the EDS elemental map of Fe.) and (g) IFIP/FeOOH/aPP membranes (The inset picture (2 μm × 2 μm) is the amplified SEM image, where nanorods morphology is marked in blue.).

Particularly, porous FeOOH has attracted extensive attention thanks to its nanoporous structure and ultra-high porosity (BET: 29.67 m^2/g, average pore size: 2.8 nm) [25,26], as well as its facile sysnthesis process and physicochemical stability. Zhang et al. [27] constructed the interlayer by vacuum filtration of pre-synthesized α-FeOOH nanorods on PES microfiltration membrane to improve the separation performance of TFC membranes. The resulting TFC membranes exhibited a high water permeability (34.1 $L{\cdot}m^{-2}{\cdot}h^{-1}{\cdot}bar^{-1}$), high rejection for Na_2SO_4 (95.0 %). In recent years, the nanoparticle interlayer constructed by in situ synthesis method is considered to be an effective means to solve the problem of agglomeration of nanomaterials during preparation and the gradual disappearance of nanoparticles during use due to their controllability, uniformity and stability [28]. At present, in-situ synthesized FeOOH functionalized membranes were mainly used in the removal of large molecular organics in the field of water treatment [29] and the field of oil-water separation [30].

To overcome these challenges, here we developed a TFC membrane with robust nanorod interlayer for ultrafast precision sieving. The high-performance interlayer enhanced TFC (i-TFC) membrane was fabricated by synthesizing a thin polyamide film on the rigid interlayer composed of FeOOH nanorods. The water permeance, salt rejection, as well as the pressure resistance and antifouling properties of the i-TFC membranes were studied and compared with the state-of-the-art nanofiltration membranes. Furthermore, the versatility of the fabrication route was demonstrated with a variety of non-polar substrates (polyethylene (PE), polypropylene (PP) and polytetrafluoroethylene (PTFE) membranes).

2. Methods

2.1. Fabrication of FeOOH functionalized interlayer

The synthesis process of FeOOH was shown in Fig. 1. Firstly, the amine functionalized polypropylene membranes (0.14 m × 0.1 m) were fabricated by coating the diazo salt solution. The preparation of the diazo salt solution and the mechanism of the modification is shown in Fig. S1. Subsequently, the modified PP membranes were thoroughly rinsed with deionized water and designated as aPP stored in deionized water. The synthesis process of FeOOH was prepared as follows: in a nutshell, 25 mL HCl (pH 2) solution and 0.57 g $FeCl_3$ were dissolved into 50 mL deionized water forming a clear synthesis solution. Then the aPP substrates were fixed by polymethyl methacrylate frames with the surface layer up. Then aPP substrates were coated by the clear synthesis solution. Finally, the above frames were sealed with a polymethyl methacrylate plate and placed in the 60 °C ovens at various times (2 h, 6 h, 10 h and 14 h). The obtained modified substrates were thoroughly rinsed with deionized water and marked as FeOOH-2h/aPP, FeOOH-6h/aPP, FeOOH-10h/aPP and FeOOH-14h/aPP. In further brief, the FeOOH-10h/aPP substrate was also abbreviated as FeOOH/aPP.

2.2. Fabrication of i-TFC membranes by the IFIP

The piperazine (PIP) monomer in the aqueous phase reacts with the acyl chloride (TMC) monomer in the organic phase to form a homogeneous polyamide layer. The typical fabrication of i-TFC (IFIP/FeOOH/aPP) membranes by the in-situ free interface polymerization (IFIP) based on our previous work was as follows [31]. the modified substrates were immersed into the 0.025 wt% PIP aqueous solutions for 1 min. When the modified polypropylene substrates were taken out from the aqueous solution, which can be wetted completely to make a continuous water-course. Then, they were fixed by frames with the surface layer up and put into the chamber full of organic solution microdroplets (0.05 % wt% TMC/hexane solution) for 60 s (Fig. S5). Then, polymerization reaction occurs at a uniform oil-water interface. Subsequently, the resulting membrane was transferred to an oven at 60 °C to dry the solvent and cure for 5 min. According to reports, the separation performance of polyamide NF membranes can be enhanced by solvent activation [32,33]. The fabricated IFIP/FeOOH/aPP membranes were immersed in DMSO at 20 °C for 20 min and then washed with deionized water. NF membranes fabricated by conventional IP on different substrates are marked as IP/FeOOH/aPP or IP/aPP.

2.3. Membrane characterization

The chemical components of various substrates and TFC membranes were characterized through X-ray photoelectron spectroscopy (XPS, Quanta200 spectrometer, USA) and Attenuated Total Reflectance-Fourier Transform Infrared Spectroscopy (ATR-FTIR, Thermo-Fisher Nicolet iS10, USA). The surface and cross-sectional images of the various membranes were characterized by Scanning electron microscope (SEM, JEOL 7900F, Japan). For cross-sectional studies, the membranes were prepared by cracked in liquid nitrogen and freeze-drying. Transmission electron microscopy (TEM, JEM 1200EX, JEOL, Japan) was also conducted to analyse the cross-section morphology. The energy dispersive spectrometer (EDS, FEI Quanta FEG 250, USA) was used to analyse the surface element distribution of the FeOOH/aPP. The surface roughness, the Young's modulus and the surface area were characterized by Atomic force microscopy (AFM, Shimadzu SPM-9700, Japan). The membrane hydrophilicity was characterized by measuring the water contact angle (DSA30, Kruss GmbH, Germany) of the supports under room temperature (25 °C). The surface charge of various substrates at different pH conditions (pH was adjusted from 3.0 to 10.0 by using HCl and NaOH solution) was measured by using the ζ potential analyzer (SurPASSTEM3, AatonPaar, Austria). Crystal structures of the aPP membrane and in situ-synthesized FeOOH nanocrystals were acquired by X-ray diffraction patterns (XRD, PANalytical B.V., Netherlands). The electronic tensile tester was applied to measure the tensile strength of the PP membranes (HY-0580, Shanghai Hengyi Testing Instruments Co.LTD.).

2.4. Separation performance of the i-TFC membrane

The water flux and different inorganic salts rejections of various membranes were tested in a cross-flow system under the pressure of 4 bar with the effective test area (A) of 18.5 cm^2 at 25 °C for 2000 ppm for all feed concentrations. Before the test, all membranes were pre-compacted for 1 h to ensure steady-state. The rejection of TFC membrane can be obtained by the following equation:

$$\text{Rejection}\ (\%) = \left(1 - C_p/C_f\right) \times 100\%. \quad (1)$$

For inorganic salts, C_f and C_p represent the concentrations of the feed solution and permeate, which is determined by measuring the conductivity.

The permeance (P) is calculated from the equation:

$$P\ \left(L{\cdot}m^{-2}{\cdot}h^{-1}{\cdot}bar^{-1}\right) = V/(AtΔP). \quad (2)$$

where V is the solvents volume of permeate, ΔP is transmembrane pressure and t represents the specified time.

3. Results and discussion

3.1. Fabrication and characterization of FeOOH nanorod interlayered TFC membranes

The fabrication of i-TFC membrane is schematically shown in Fig. 1a. The commercial non-polar polypropylene (PP) was selected as the support because of its high solvent resistance, excellent mechanical strength, high porosity and low cost. To enhance the adhesive force between the FeOOH nanorods and the PP support, we functionalized the PP substrate with amino groups (named as aPP) by grafting a polyaminophenylene (PAP) layer on top, since —NH_2 can act as ligands for binding Fe (Fig. S1) [24,29]. Compared with the pristine PP, two new

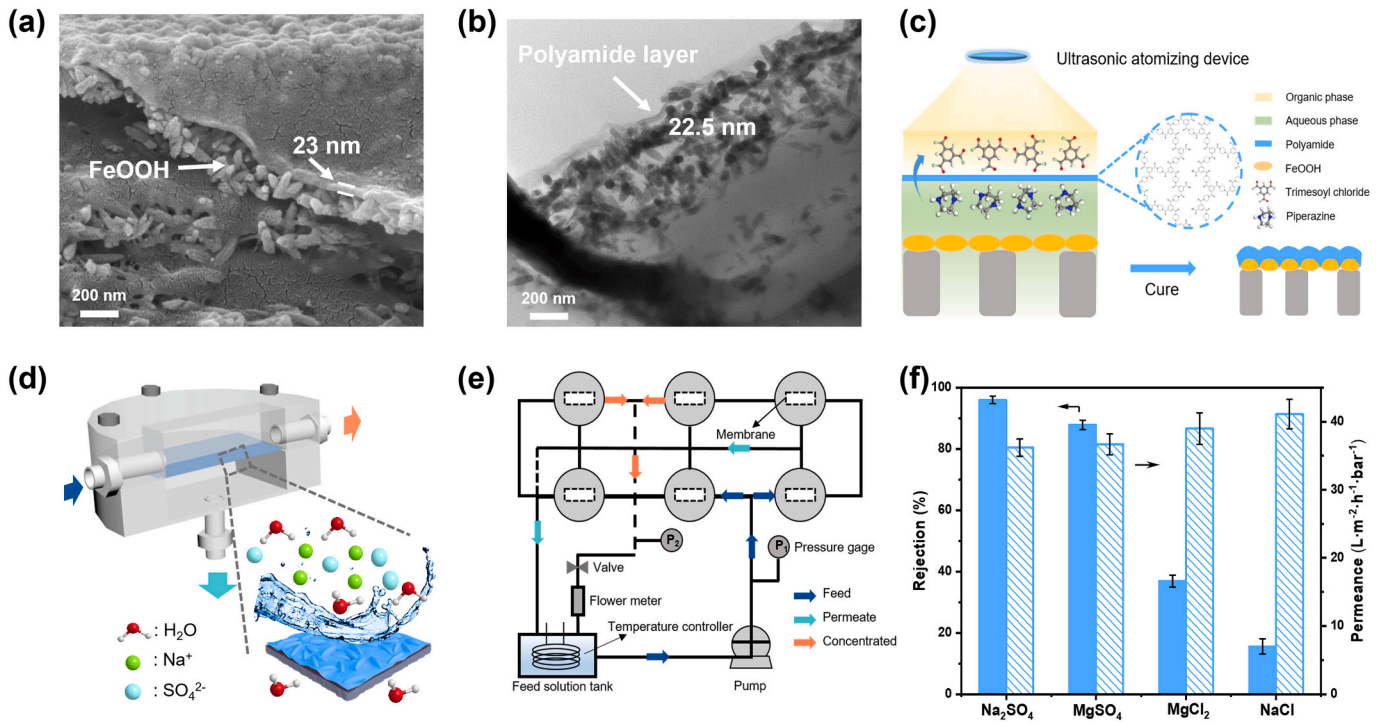

Fig. 2. Cross-sectional SEM (a) and TEM (b) images of the IFIP/FeOOH/aPP membrane. (c) The in-situ free interface polymerization (IFIP) scheme for preparing an i-TFC membrane. (d) Schematic illustration of the home-made permeation cell (test area up to 18.5 cm^2) and the separation mechanism of the membrane. (e) Diagram of the cross-flow filtration apparatus composed of six permeation cells (operation pressure = 4.0 bar, cross-flow rate = 4.5 $L{\cdot}min^{-1}$). (f) NF performance of IFIP/FeOOH/aPP membrane toward different inorganic salts.

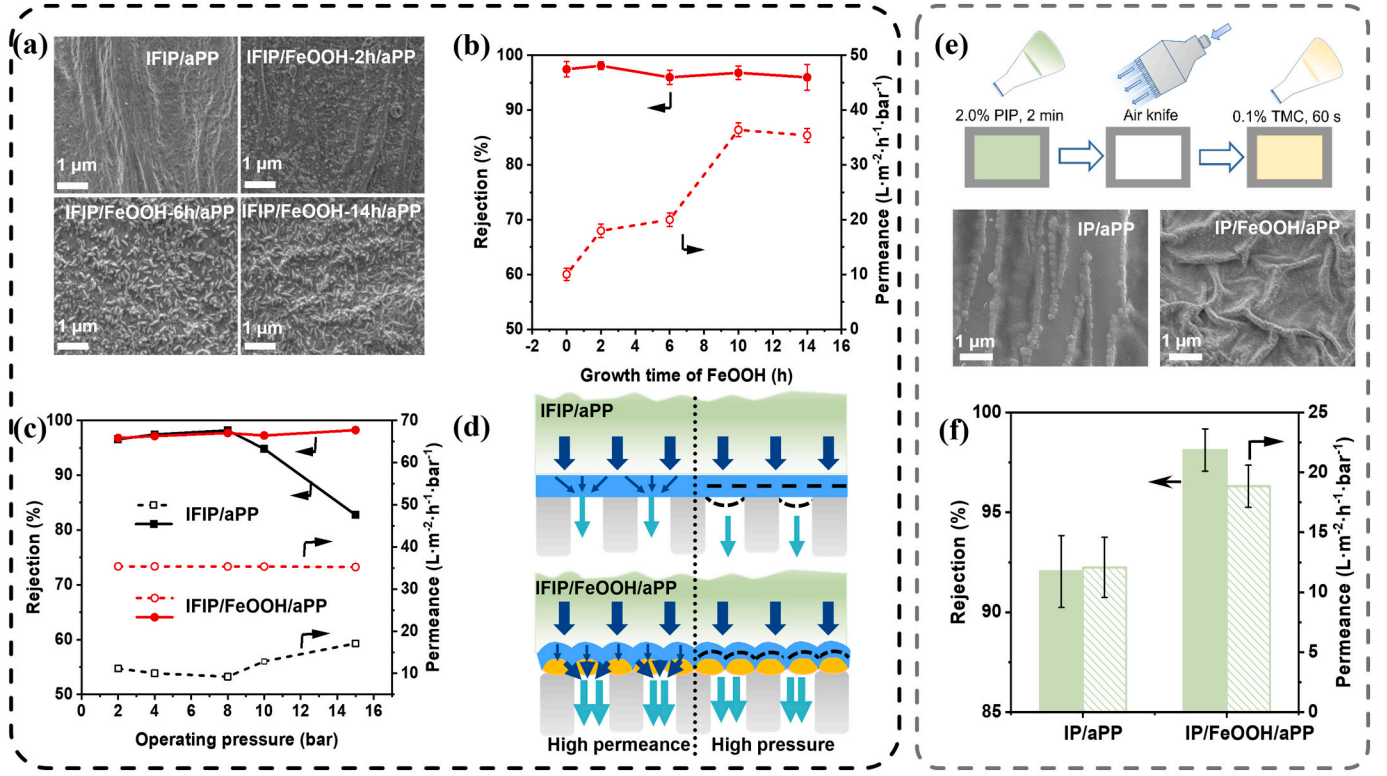

Fig. 3. (a) SEM topography images of IFIP/aPP, IFIP/FeOOH-2h/aPP, IFIP/FeOOH-6h/aPP and IFIP/FeOOH-14h/aPP. (b) Effect of introducing FeOOH interlayer with different synthesis times on nanofiltration performance. (c) The pressure resistance of the IFIP/aPP and IFIP/FeOOH/aPP (IFIP/FeOOH-10h/aPP) membranes. (d) Schematic diagrams of water transport path and micro-deformation (dotted line) of polyamide layer of IFIP/aPP and IFIP/FeOOH/aPP membrane under pressure. (e) Schematic illustration of the traditional interfacial polymerization (IP) preparation process and SEM topography images of IP/aPP and IP/FeOOH/aPP membranes. (f) The Na2SO4 rejection and the permeance of IP/aPP and IP/FeOOH/aPP membranes.

peaks were detected at 1622 cm^{-1} and 1515 cm^{-1} in the ATR-FTIR spectra for the aPP substrate, assigned to the —NH_2 groups and benzene ring stretching vibrations (Fig. 1b). XPS analysis also confirmed the presence of —N═N— and —NH_2 functional groups on the aPP surface (Figs. 1c and S2).

The FeOOH was then grown on the aPP substrate by dipping the substrate into the precursor solution and annealing it at 60 °C. Two typical vibration peaks at 841 cm^{-1} (Fe—O) and 690 cm^{-1} (Fe—O—Fe), as well as a broad peak ranging from 3000 to 3600 cm^{-1} attributed to the stretching vibration of —OH, were observed for the FeOOH coated substrate (Fig. 1b). The presence of FeOOH also induced a red shift of the —NH_2 peaks [28]. XPS analysis also demonstrated the existence of Fe 2p and O1s (Figs. 1c and S3). The diffraction peaks located at 12°, 26.9°, 34.1°, 35.3°, 39.4°, 46.6° and 56.2° correspond to the (110), (310), (400), (211), (301), (411) and (521) crystal planes of β-FeOOH (JCPDS No. 34-1266) (Fig. 1d) [34], indicating the crystalline structure of the interlayer. According to the SEM imaging, the FeOOH crystals were grown in the form of nanorods and were evenly distributed on the porous aPP substrate (Fig. 1e-f). We found that the areal density of the FeOOH nanorods increased with the growth time and achieved a complete surface coverage after 10 h reactions (Fig. S4). The energy dispersive spectrum demonstrated a uniform distribution of the Fe element on the substrate (Fig. 1f).

Eventually, a 23-nm-thick polyamide film was fabricated on the FeOOH nanorod interlayer by in-situ free interface polymerization (IFIP) which can avoid the manual transfer step and enable a reduction of the film thickness (Figs. 1g and 2a-b) [31]. The microcopy imaging showed that the polyamide film followed the topography of the underlying nanorods, indicating a strong adhesion between the polyamide film and the nanorode interlayer. The strong interaction between the nanorod interlayer and the polyamide layer originates from two sources. On the one hand this may be due to the increased surface roughness after the formation of FeOOH nanorods to increase the adhesion area and physical adhesion between the support and the active layer [35]. In addition, the abundance of hydroxyl groups on the surface of the FeOOH nanorods and the amine groups on the surface of the support increased the covalent or ionic bonding interaction with the active layer [36]. In the IFIP process, an ultrasonic atomizing device was utilized to generate organic phase microdroplets to prevent the formation of defects (Fig. S5 and Fig. 2c). A characteristic peak of amide group at 1630 cm^{-1} was observed in the ATR-FTIR spectra, demonstrating the formation of polyamide on the substrates (Fig. S6).

The performance of the i-TFC membrane was tested in a cross-flow permeation cell for filtration of different inorganic salts (Fig. 2d-e). According to Zeta potential measurements, the membrane displayed an isoelectric point at pH of 3.5, suggesting that negative charges are dominant on the membrane surface in neutral solutions (Fig. S7). The permeation experiments showed that the membrane suppressed the passage of salts with divalent anions (SO_4^{2-}) more strongly than monovalent ones (Cl^-), which was thus assigned to the combined effects of steric exclusion and electrostatic repulsion (Fig. 2f). Since the charges and valences of ions both contribute to ionic sieving, the salt rejection of the i-TFC membrane follow the order of $Na_2SO_4 > MgSO_4 > MgCl_2 >$ NaCl, in agreement with the sieving behavior observed by other negatively charged NF membranes [37,38]. In addition, the membrane showed a high water permeance up to 36–42 $L{\cdot}m^{-2}{\cdot}h^{-1}{\cdot}bar^{-1}$, which varied slightly among different salts that likely affected the diffusion coefficient.

3.2. Understanding the role of nanorod interlayer in separation performance

To understand the role of the nanorod interlayer in membrane separation, we prepared conventional TFC membranes using the same IFIP procedure, but without the interlayer (Fig. 3a), i.e., forming the polyamide layer directly on the pristine aPP substrate. The resulting polyamide film was neither uniform nor continuous, while the structure of the underlying PP was still clearly visible in many spots. By introducing an intermediate layer of FeOOH nanorods, the integrity and homogeneity of the film was both enhanced with the increase in the amount of nanorods. This enhancement was ascribed to the improved hydrophilicity and compactness of the substrate surface by the interlayer (Figs. S4 and S8). As the FeOOH growth time increased, more FeOOH nanorods were anchored on the support until the non-porous fibers of the support were completely covered. Compared with the pristine support with non-uniform surface porosity, the surface of the FeOOH/aPP membrane becomes more uniform and dense after the introduction of the nanorod interlayer. The water contact angle was reduced from 67.9° to 45.8° due to the introduction of —OH groups from FeOOH, which will facilitate the uniform spreading of the aqueous monomer solution in the synthesis procedure of polyamide layers, resulting in smooth and defect-free thin films.

The NF experiments showed that the water permeance increased significantly with the amount of FeOOH, and started to saturate when the nanorods were grown for 10 h, reaching up to 36.4 $L{\cdot}m^{2}{\cdot}h^{-1}{\cdot}bar^{-1}$, which is about 3.6 times that of the pristine IFIP/aPP membrane (Fig. 3b). Meanwhile, these membranes remained a high rejection of Na_2SO_4 above 96 %. These results suggested that the porous interlayer provides efficient transport channels for the composite membrane, enabling the rapid transport of water molecules between the support and the polyamide layer [24]. Besides, the nanorod morphology also increases the effective mass transport area of the composite membrane. Furthermore, the mechanical strength of the nanocomposite membrane was also greatly enhanced by the nanorods, based on the pressure resistance experiments (Fig. 3c). The rejection rate of the IFIP/aPP membrane dropped instantly when the applied pressure was above 8 bar, likely due to the deformation and cracking of the polyamide layer caused by the high pressure (Fig. S9). In contrast, the IFIP/FeOOH/aPP membrane remained high salt rejection rates at pressures up to 15 bar, indicating that the FeOOH nanorods function as a robust interlayer to protect the thin polyamide film (Fig. 3d). The tensile strength (Table S1) and Young's modulus (Fig. S10) of the membranes were significantly increased by the introduction of FeOOH compared to the pristine membrane, and the Young's modulus of the prepared IFIP/FeOOH/aPP membrane was also significantly increased due to the enhanced rigidity of the support layer. Combined with mechanical characterization and pressure resistance experiments, it was shown that the mechanical properties of TFC membranes were significantly improved after the introduction of FeOOH. There are two potential reasons for this optimized mechanism. On the one hand, the introduction of the FeOOH interlayer optimized the pore structure on the surface of the base film, resulting in a better pressure resistance of the TFC membrane compared to the large pore structure on the surface of the original membrane, which caused the top polyamide layer to undergo destructive deformation when subjected to high pressure [39]. On the other hand, after the introduction of the FeOOH interlayer, the mechanical stability of the polymer is maintained due to the chemical bonds and spatial stabilizing force between the support and the FeOOH interlayer [40]. A large number of studies have shown that the “membrane compaction” effect of the TFC membrane can be improved by improving the mechanical properties of the skin layer of the support, thereby enhancing the mechanical strength of the composite membrane [18]. As shown in Fig. S11, the membrane depicted good long-term stability during the test. It can also be seen from Fig. S12 that the tested IFIP/FeOOH/aPP film still has a stable nanorod interlayer as well as a defect-free polyamide layer.

The antifouling performance of the IFIP/FeOOH/aPP membrane was also improved after the introduction of FeOOH (Fig. S13). This can be rationalized by characterizing surface charge and surface hydrophilicity. It can be seen from Fig. S14 (a) that the isoelectric point of the IFIP/FeOOH/aPP film (3.52) is lower than that of the initial TFC film (4.12) due to the introduction of hydroxyl-rich FeOOH. This causes the

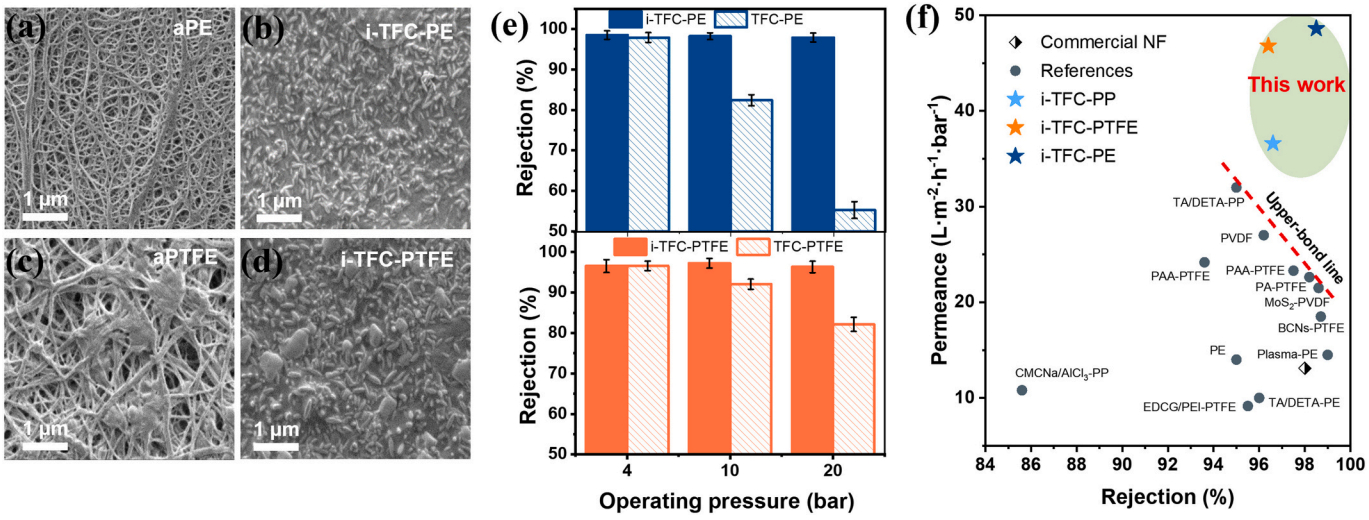

Fig. 4. SEM topography images of (a) aPE, (b) IFIP/FeOOH/aPE, (c) aPTFE and (d) IFIP/FeOOH/aPTFE membranes. (e) The Na_2SO_4 rejection of various NF membranes under different operating pressure. (f) Comparison of water permeance and Na_2SO_4 rejection achieved by this work and other NF membranes fabricated on various non-polar substrates reported in the literature.

membrane surface to exhibit a stronger negative charge, which will enhance the electrostatic repulsion of the negatively charged contaminant BSA. At the same time, the IFIP/FeOOH/aPP membrane has a smaller contact angle, which will further reduce the adsorption of pollutants.

In addition, we also prepared and tested the IP/aPP and IP/FeOOH/aPP membranes by conventional interfacial polymerization (IP) (Fig. 3e). Similarly, the presence of the nanorod interlayer reduced the formation of defects in the polyamide layer (Fig. 3e), and enhanced the water permeance and Na_2SO_4 rejection (Fig. 3f). Compared with the IFIP/FeOOH/aPP membrane fabricated by IFIP, the water permeance of the conventional IP membrane (IP/FeOOH/aPP) was reduced by half due to the increased thickness (34.7 nm) of the polyamide layer (Fig. S10).

3.3. The versatility of the interlayer and comparison with state-of-the-art

The versatility of the fabrication scheme was demonstrated by fabricating the i-TFC membranes on different non-polar polymer substrates, such as PE and PTFE (Fig. 4a-d). The rejection of Na_2SO_4 by i-TFC membranes all exceeds 98 %. Among these membranes, the i-TFC-PE membrane showed the highest water permeance, up to 48.94 $L{\cdot}m^{-2}{\cdot}h^{-1}{\cdot}bar^{-1}$ (Fig. S21), which was ascribed to the higher porosity and larger pores of the PE support (Table S2). In addition, the i-TFC membranes can always withstand higher pressures than the TFC membranes prepared without the interlayer, regardless of the support type (Fig. 4e). When the applied pressure was increased to 20 bar, the rejection of Na_2SO_4 remained above 96 % for i-TFC membranes, while the rejection for TFC membranes dropped instantly below 80 %. In particular, the rejection of TFC-PE membrane was reduced to only 50 % at 20 bar, because the bigger pores and higher porosity of PE cannot provide sufficient mechanical strength for the polyamide membrane under high pressures. The i-TFC membranes obtained from this work were also compared with other state-of-the-art interlayer enhanced TFC membranes that were prepared on non-polar substrates (Fig. 4f) [32,41–50]. We found that the nanorod interlayered-TFC membranes outperform the other reported i-TFC membranes with regards to water permeance and salt rejection, which can be attributed to the high porosity of the FeOOH nanorods and the intactness of the thin polyamide film.

4. Conclusions

In summary, high-performance nanorod interlayered i-TFC membranes were fabricated on commercial hydrophobic substrates (PP, PE and PTFE) by in-situ free interfacial polymerization. These i-TFC membranes outperform the conventional TFC membranes in terms of water permeance, mechanical strength, and anti-fouling performance, attributed to the presence of the porous, robust and hydrophilic FeOOH nanorods. The resulting i-TFC membranes showed high water permeance up to 48.9 $L{\cdot}m^{-2}{\cdot}h^{-1}{\cdot}bar^{-1}$ while maintaining high Na_2SO_4 rejection of 98.6 %, which effectively overcome the typical trade-off effect. The fabrication strategy of the nanorod i-TFC membrane provides an effective means to develop high-performance NF membranes with broad application prospects, such as organic solvent nanofiltration in harsh organic media.

CRediT authorship contribution statement

Pengfei Li: Visualization, Conceptualization, Methodology, Experiment, Software, Data curation, Writing - Original draft preparation, Writing- Reviewing and Editing.

Bingxin Wei: Visualization, Experiment and Software.

Zhen Yao: Software.

Peng Li: Validation, Supervision.

Yingfei Hou: Conceptualization, Resources and Methodology.

Yang Yang: Review & editing.

Q. Jason Niu: Supervision, Funding acquisition, Writing - review & editing.

Declaration of competing interest

The authors declare that they have no known competing financial interests or personal relationships that could have appeared to influence the work reported in this paper.

Data availability

No data was used for the research described in the article.

Acknowledgements

We gratefully acknowledge the National Science Foundation of

China (No. U2006230) and China Scholarship Council (No. 202106450052).

Appendix A. Supplementary data

Supplementary data to this article can be found online at https://doi.org/10.1016/j.desal.2022.116255.

References

[1] Y. Yang, P. Dementyev, N. Biere, D. Emmrich, P. Stohmann, R. Korzetz, X. Zhang, A. Beyer, S. Koch, D. Anselmetti, A. Golzhauser, Rapid water permeation through carbon nanomembranes with sub-nanometer channels, ACS Nano 12 (2018) 4695–4701.

[2] Y.Q. Zhang, J. Guo, G. Han, Y.P. Bai, Q.C. Ge, J. Ma, C.H. Lau, L. Shao, Molecularly soldered covalent organic frameworks for ultrafast precision sieving, Sci. Adv. 7 (2021).

[3] Z. Tan, S. Chen, X. Peng, L. Zhang, C. Gao, Polyamide membranes with nanoscale Turing structures for water purification, Science 360 (2018) 518–521.

[4] G.M. Shi, Y.N. Feng, B.F. Li, H.M. Tham, J.Y. Lai, T.S. Chun, Recent progress of organic solvent nanofiltration membranes, Prog. Polym. Sci. 123 (2021), 101470.

[5] J.R. Werber, C.O. Osuji, M. Elimelech, Materials for next-generation desalination and water purification membranes, Nat. Rev. Mater. 1 (2016) 16018.

[6] H.B. Park, J. Kamcev, L.M. Robeson, M. Elimelech, B.D. Freeman, Maximizing the right stuff: the trade-off between membrane permeability and selectivity, Science 356 (2017) 6343.

[7] S.P. Nunes, P.Z. Culfaz-Emecen, G.Z. Ramon, T. Visser, G.H. Koops, W.Q. Jin, M. Ulbricht, Thinking the future of membranes: perspectives for advanced and new membrane materials and manufacturing processes, J. Membr. Sci. 598 (2020), 117761.

[8] R. Epsztein, R.M. DuChanois, C.L. Ritt, A. Noy, M. Elimelech, Towards single-species selectivity of membranes with subnanometre pores, Nat. Nanotechnol. 15 (2020) 426–436.

[9] R. Shevate, D.L. Shaffer, Large-area 2D covalent organic framework membranes with tunable single-digit nanopores for predictable mass transport, ACS Nano 16 (2022) 2407–2418.

[10] Z. Liu, Z. Ma, B. Qian, A.Y.H. Chan, X. Wang, Y. Liu, J.H. Xin, A facile and scalable method of fabrication of large-area ultrathin graphene oxide nanofiltration membrane, ACS Nano 15 (2021) 15294–15305.

[11] S. Karan, Z. Jiang, A.G. Livingston, Sub–10 nm polyamide nanofilms with ultrafast solvent transport for molecular separation, Science 348 (2015) 1347–1351.

[12] L. Long, C. Wu, Z. Yang, C.Y. Tang, Carbon nanotube interlayer enhances water permeance and antifouling performance of nanofiltration membranes: mechanisms and experimental evidence, Environ. Sci. Technol. 56 (2022) 2656–2664.

[13] K. Wang, X. Wang, B. Januszewski, Y. Liu, D. Li, R. Fu, M. Elimelech, X. Huang, Tailored design of nanofiltration membranes for water treatment based on synthesis-property-performance relationships, Chem. Soc. Rev. 51 (2022) 672–719.

[14] X. Wu, M. Ding, H. Xu, W. Yang, K. Zhang, H. Tian, H. Wang, Z. Xie, Scalable Ti3C2Tx MXene interlayered forward osmosis membranes for enhanced water purification and organic solvent recovery, ACS Nano 14 (2020) 9125–9135.

[15] Y.F. Hao, Q. Li, B.Q. He, B. Liao, X.H. Li, M.Y. Hu, Y.H. Ji, Z.Y. Cui, M. Younas, J. X. Li, An ultrahighly permeable-selective nanofiltration membrane mediated by an in situ formed interlayer, J. Mater. Chem. A 8 (2020) 5275–5283.

[16] S. Gao, Y. Zhu, Y. Gong, Z. Wang, W. Fang, J. Jin, Ultrathin polyamide nanofiltration membrane fabricated on brush-painted single-walled carbon nanotube network support for ion sieving, ACS Nano 13 (2019) 5278–5290.

[17] M.Y. Wu, J.Q. Yuan, H. Wu, Y.L. Su, H. Yang, X.D. You, R.N. Zhang, X.Y. He, N. A. Khan, R. Kasher, Z.Y. Jiang, Ultrathin nanofiltration membrane with polydopamine-covalent organic framework interlayer for enhanced permeability and structural stability, J. Membr. Sci. 576 (2019) 131–141.

[18] M.T.M. Pendergast, J.M. Nygaard, A.K. Ghosh, E.M.V. Hoek, Using nanocomposite materials technology to understand and control reverse osmosis membrane compaction, Desalination 261 (2010) 255–263.

[19] Z. Yang, P.F. Sun, X. Li, B. Gan, L. Wang, X. Song, H.D. Park, C.Y. Tang, A critical review on thin-film nanocomposite membranes with interlayered structure: mechanisms, recent developments, and environmental applications, Environ. Sci. Technol. 54 (2020) 15563–15583.

[20] C.H. Ji, Z. Zhai, C. Jiang, P. Hu, S.Z. Zhao, S.M. Xue, Z. Yang, T. He, Q.J. Niu, Recent advances in high-performance TFC membranes: a review of the functional interlayers, Desalination 500 (2021), 114869.

[21] W.F. Chan, H.Y. Chen, A. Surapathi, M.G. Taylor, X. Shao, E. Marand, J.K. Johnson, Zwitterion functionalized carbon nanotube/polyamide nanocomposite membranes for water desalination, ACS Nano 7 (2013) 5308–5319.

[22] Z. Zhai, C. Jiang, N. Zhao, W.J. Dong, H.L. Lan, M. Wang, Q.J. Niu, Fabrication of advanced nanofiltration membranes with nanostrand hybrid morphology mediated by ultrafast Noria-polyethyleneimine codeposition, J. Mater. Chem. A 6 (2018) 21207–21215.

[23] B. Yuan, S. Zhao, P. Hu, J. Cui, Q.J. Niu, Asymmetric polyamide nanofilms with highly ordered nanovoids for water purification, Nat. Commun. 11 (2020) 6102.

[24] P.F. Li, M.M. Zhang, Z. Zhai, M. Wang, P. Li, Y.F. Hou, Q.J. Niu, Precise assembly of a zeolite imidazolate framework on polypropylene support for the fabrication of thin film nanocomposite reverse osmosis membrane, J. Membr. Sci. 612 (2020).

[25] K. Gallagher, The atomic structure of tubular subcrystals of β-iron (III) oxide hydroxide, Nature 226 (1970) 1225–1228.

[26] N.T.T. Trang, L.T.M. Thy, P.M. Cuong, T.H. Tu, N.H. Hieu, Fabrication and characterization of akaganeite/graphene oxide nanocomposite for arsenic removal from water, in: AIP Conference Proceedings, AIP Publishing LLC, 2018, p. 040001.

[27] H.-Z. Zhang, Z.-L. Xu, Q. Shen, High-performance nanofiltration membrane intercalated by FeOOH nanorods for water nanofiltration, Desalination 498 (2021), 114802.

[28] Z. Zhai, N. Zhao, W. Dong, P. Li, H. Sun, Q.J. Niu, In situ assembly of a zeolite imidazolate framework hybrid thin-film nanocomposite membrane with enhanced desalination performance induced by Noria-polyethyleneimine codeposition, ACS Appl. Mater. Interfaces 11 (2019) 12871–12879.

[29] Y. Lv, C. Zhang, A. He, S.J. Yang, G.P. Wu, S.B. Darling, Z.K. Xu, Photocatalytic nanofiltration membranes with self-cleaning property for wastewater treatment, Adv. Funct. Mater. 27 (2017), 1700251.

[30] M. Wang, Z.W. Xu, Y.L. Guo, Y.F. Hou, P. Li, Q.J. Niu, Engineering a superwettable polyolefin membrane for highly efficient oil/water separation with excellent self-cleaning and photo-catalysis degradation property, J. Membr. Sci. 611 (2020), 118409.

[31] C. Jiang, L. Zhang, P. Li, H. Sun, Y. Hou, Q.J. Niu, Ultrathin film composite membranes fabricated by novel in situ free interfacial polymerization for desalination, ACS Appl. Mater. Interfaces 12 (2020) 25304–25315.

[32] M.G. Shin, S.J. Kwon, H. Park, Y.I. Park, J.H. Lee, High-performance and acid-resistant nanofiltration membranes prepared by solvent activation on polyamide reverse osmosis membranes, J. Membr. Sci. 595 (2020).

[33] M.F.J. Solomon, Y. Bhole, A.G. Livingston, High flux membranes for organic solvent nanofiltration (OSN)-interfacial polymerization with solvent activation, J. Membr. Sci. 423 (2012) 371–382.

[34] A.T. Xie, J.Y. Cui, J. Yang, Y.Y. Chen, J.D. Dai, J.H. Lang, C.X. Li, Y.S. Yan, Photo-Fenton self-cleaning membranes with robust flux recovery for an efficient oil/water emulsion separation, J. Mater. Chem. A 7 (2019) 8491–8502.

[35] Q. Shi, L. Ni, Y. Zhang, X. Feng, Q. Chang, J. Meng, Poly (p-phenylene terephthamide) embedded in a polysulfone as the substrate for improving compaction resistance and adhesion of a thin film composite polyamide membrane, J. Mater. Chem. A 5 (2017) 13610–13624.

[36] J. Peng, Y. Su, W. Chen, X. Zhao, Z. Jiang, Y. Dong, Y. Zhang, J. Liu, C. Xingzhong, Polyamide nanofiltration membrane with high separation performance prepared by EDC/NHS mediated interfacial polymerization, J. Membr. Sci. 427 (2013) 92–100.

[37] Z.L. Qiu, L.F. Fang, Y.J. Shen, W.H. Yu, B.K. Zhu, C. Helix-Nielsen, W. Zhang, Ionic dendrimer based polyamide membranes for ion separation, ACS Nano 15 (2021) 7522–7535.

[38] H. Peng, W.H. Zhang, W.S. Hung, N. Wang, J. Sun, K.R. Lee, Q.F. An, C.M. Liu, Q. Zhao, Phosphonium modification leads to ultrapermeable antibacterial polyamide composite membranes with unreduced thickness, Adv. Mater. 32 (2020), e2001383.

[39] Z. Yang, Z.-W. Zhou, H. Guo, Z. Yao, X.-H. Ma, X. Song, S.-P. Feng, C.Y. Tang, Tannic acid/Fe3+ nanoscaffold for interfacial polymerization: toward enhanced nanofiltration performance, Environ. Sci. Technol. 52 (2018) 9341–9349.

[40] H. Chen, Q. Lin, Q. Xu, Y. Yang, Z. Shao, Y. Wang, Plasma activation and atomic layer deposition of TiO2 on polypropylene membranes for improved performances of lithium-ion batteries, J. Membr. Sci. 458 (2014) 217–224.

[41] H.Y. Tang, J. He, L.T. Hao, F. Wang, H.P. Zhang, Y.H. Guo, Developing nanofiltration membrane based on microporous poly(tetrafluoroethylene) substrates by bi-stretching process, J. Membr. Sci. 524 (2017) 612–622.

[42] X.P. Wang, Q. Xiao, C. Wu, P. Li, S.J. Xia, Fabrication of nanofiltration membrane on MoS2 modified PVDF substrate for excellent permeability, salt rejection, and structural stability, Chem. Eng. J. 416 (2021), 129154.

[43] J.H. Wu, M.J. Xia, Z.W. Li, L.G. Shen, R.J. Li, M.J. Zhang, Y. Jiao, Y.C. Xu, H.J. Lin, Facile preparation of polyvinylidene fluoride substrate supported thin film composite polyamide nanofiltration: effect of substrate pore size, J. Membr. Sci. 638 (2021), 119699.

[44] N. Zhang, Z.H. Huang, N. Yang, L.H. Zhang, B. Jiang, Y.L. Sun, J.W. Ma, Nanofiltration membrane via EGCG-PEI co-deposition followed by cross-linking on microporous PTFE substrates for desalination, Sep. Purif. Technol. 232 (2020), 115964.

[45] S. Wang, Z.Y. Wang, J.Z. Xia, X.M. Wang, Polyethylene-supported nanofiltration membrane with in situ formed surface patterns of millimeter size in resisting fouling, J. Membr. Sci. 620 (2021).

[46] S.C. Yu, Y.P. Zheng, Q. Zhou, S. Shuai, Z.H. Lu, C.J. Gao, Facile modification of polypropylene hollow fiber microfiltration membranes for nanofiltration, Desalination 298 (2012) 49–58.

[47] X. Zhang, C. Liu, J. Yang, C.Y. Zhu, L. Zhang, Z.K. Xu, Nanofiltration membranes with hydrophobic microfiltration substrates for robust structure stability and high water permeation flux, J. Membr. Sci. 593 (2020) 0376–7388.

[48] C. Shang, L. Wang, J. Xia, S. Zhang, Macropatterning of microcrumpled nanofiltration membranes by spacer imprinting for low-scaling desalination, Environ. Sci. Technol. 54 (2020) 15527–15533.

[49] Y. Zong, R.J. Zhang, S.S. Gao, H.L. Chang, B. Van der Bruggen, J.Y. Tian, Anti-drying nanofiltration (NF) membranes constructed on PTFE microfiltration (MF) substrate via novel interfacial polymerization, J. Membr. Sci. 638 (2021) 0376–7388.

[50] X.X. Teng, W.X. Fang, Y.Z. Liang, S.H. Lin, H.Z. Lin, S.S. Liu, Z.Y. Wang, Y.Z. Zhu, J. Jin, High-performance polyamide nanofiltration membrane with arch-bridge structure on a highly hydrated cellulose nanofiber support, Sci. China Mater. 63 (2020) 2570–2581.